Separation and Purification Technology 210 (2019) 242–250

Contents lists available at ScienceDirect

Separation and Purification Technology

journal homepage: www.elsevier.com/locate/seppur

The role of *ortho*-, *meta*- and *para*-substitutions in the main-chain structure of poly(etherimide)s and the effects on CO_2/CH_4 gas separation performance

Zeljka P. Madzarevic[a,b], Salman Shahid[c,d], Kitty Nijmeijer[d,e], Theo J. Dingemans[a,f,*]

[a] Faculty of Aerospace Engineering, Delft University of Technology, Kluyverweg 1, 2629HS Delft, The Netherlands
[b] Dutch Polymer Institute (DPI), P.O. Box 902, 5600AX Eindhoven, The Netherlands
[c] Centre for Advanced Separations Engineering, University of Bath, Bath BA2 7AY, United Kingdom
[d] Membrane Science and Technology, MESA+ Institute for Nanotechnology, University of Twente, Meander, ME 325, PO Box 217, 7500AE Enschede, The Netherlands
[e] Membrane Materials and Processes, Eindhoven University of Technology, Department of Chemical Engineering and Chemistry, P.O. Box 513, 5600MB Eindhoven, The Netherlands
[f] University of North Carolina at Chapel Hill, Department of Applied Physical Sciences, Murray Hall 1113, 121 South Road, NC 27599-3050, USA

ARTICLE INFO

Keywords:
Polyetherimide membranes
CO_2 removal
Structure-property relationship
Plasticization
Gas separation

ABSTRACT

A homologous series of 12 all-aromatic PEI membranes was investigated with the aim to understand how subtle changes in the PEI main-chain affect the carbon dioxide/methane (CO_2/CH_4) gas separation performance. The 3-ring diamines selected for this study are either *para*-, *meta*- or *ortho*-aryloxy substituted with respect to the central benzene ring, *i.e.* 1,4-bis(4-aminophenoxy)benzene (P1), 1,3-bis(4-aminophenoxy)benzene (M1) and 1,2-bis(4-aminophenoxy)benzene (O1). Doing so changes the backbone geometry from a more linear to a more kinked conformation. In addition, four dianhydrides were selected with the aim to tailor the segmental mobility and hence the free volume of the PEIs, *i.e.* pyromellitic dianhydride (**PMDA**), 3,3′,4,4′-biphenyltetracarboxylic dianhydride (**BPDA**), 3,3′,4,4′-benzophenonetetracarboxylic dianhydride (**BTDA**) and 3,3′,4,4′-oxydiphthalic dianhydride (**ODPA**). We have investigated how subtle changes in these prototypical PEIs affect membrane critical performance criteria such as CO_2 permeability, CO_2/CH_4 selectivity and ability to withstand high operating pressures. In ODPA-based membranes the CO_2 permeability decreases in the order P1 > O1 > M1 and remains steady throughout measurements with mixed feed pressures up to 40 bar, however, the selectivity decreases for ODPA-O1 and ODPA-M1. For high-pressure applications, the OPDA-P1 membrane is a good candidate with a selectivity of 48, permeability of CO_2 of 0.74 Barrer and ability to resist plasticization up to 40 bar of total pressure (16 bar of CO_2 partial pressure). Alternatively, for applications up to 10 bar of total mixed feed (5 bar of CO_2 partial pressure), BPDA-O1 is a promising candidate because this membrane displays a high selectivity of 70 and permeability of 1.3 Barrer.

1. Introduction

Membrane-based gas separation is an important unit operation in many industrial processes and is gaining momentum in natural gas upgrading [1], carbon dioxide removal from flue gas [2], biogas purification [3] and landfill gas treatment. Sources of natural gas with higher concentrations of CO_2 are being explored since the sources of low carbon dioxide (CO_2) containing natural gas are limited and all but exhausted. CO_2 reduces the heating value of methane gas streams and causes corrosion in pipelines and equipment [4], so it is important to remove CO_2 from natural gas prior to use. Separation of CO_2 using polymer-based membranes is a competitive alternative with respect to conventional absorption technologies such as amine scrubbing [5] owing to its high energy efficiency, simple design (easy scale-up), and high area-to-volume ratio (compactness) [6]. In order to have the desired robustness and membrane lifetime the polymers used for these membranes need to exhibit high flux and high selectivity, and from the material selection point of view, they need to meet the following requirements: chemical and thermal resistance, good mechanical properties, plasticization resistance and physical aging tolerance [2].

A great deal of research has been done to improve the gas permeability and selectivity for polymer membranes, with the main focus being on the relationship between the polymer backbone structure and the gas separation properties. The gas permeation properties of glassy

* Corresponding author at: University of North Carolina at Chapel Hill, Department of Applied Physical Sciences, Murray Hall 1113, 121 South Road, NC 27599-3050, USA.
E-mail address: tjd@unc.edu (T.J. Dingemans).

https://doi.org/10.1016/j.seppur.2018.08.006
Received 25 June 2018; Received in revised form 4 August 2018; Accepted 4 August 2018
Available online 07 August 2018
1383-5866/

polymers are very sensitive to the chemical structure of the repeating units [7], with their chains having restricted mobility below the glass transition temperature. It has been reported that an increase in backbone rigidity improves selectivity since it helps molecular sieving of gases with similar solubility coefficients [8]. However, this also results in a decrease in permeability. Most of the polymers that have been investigated typically show the general trend that highly permeable polymers possess rather low selectivity and *vice versa*, which is referred to as the permeability/selectivity trade-off relationship [9,10]. The most studied class of polymers for membrane materials for gas separation are polyimides (PIs) and poly(etherimide)s (PEIs) [11]. Both PIs and PEIs are known for their high thermal and mechanical stability.

Commercial PIs for gas separation are known under trade names such as Upilex® and Matrimid®. The later has been extensively studied owing to a combination of properties, for CO_2/CH_4 gas separation at 10 bar, it shows a selectivity of 34 and permeability of CO_2 of 6.5 Barrer [12]. However, with increased CO_2 partial pressure the selectivity coefficient drops, the permeability of the slower gas is enabled by the highly soluble, faster gas. This is attributed to the plasticization effects, caused by the high CO_2 solubility and its interaction with the polyimide membrane. As the membrane is plasticized, the permeability increases significantly, while the selectivity decreases [13–15]. Plasticization is a common problem in polyimide- and polyetherimide-based membranes. If this issue could be resolved, PIs and PEIs could become potential candidates for high-pressure CO_2/CH_4 gas separation applications.

A number of techniques has been reported in literature to improve PI and PEI membranes both in plasticization resistance and in increasing permeability. One such technique is via cross-linking. This has been shown to be an effective method to improve membrane stability, specifically referring to plasticization as well as physical aging, but it comes at cost of low permeability [16,17]. Another method to improve permeability is the introduction of bulky groups on the polymer backbone. They help to disrupt chain packing, which in turn results in an increase in free volume [18] *e.g.* the presence of bulky $–CF_3$ groups in 6FDA-durene leads to very high permeability values (678 Barrer) but low selectivity values of ~20 [19]. When evaluating the available literature, it is clear that a wide variety of PI- and PEI-backbone modifications have been explored. Work of Ayala *et al.* shows that gas permeability typically increases with increasing free volume, and free volume could be related to the chemical composition of the polymer backbone and to the nature of the pendant groups [20]. However, what seems to be missing is a basic understanding of how subtle systematic changes in the PEI main-chain affect the gas separation performance. A start was made by Simons et al. [21] They showed that, under conditions where commercial membranes suffer from plasticization, 3,3′,4,4′-oxydiphthalic dianhydride (ODPA) based PEIs are promising membranes that show increasing CO_2 sorption with increasing T_g. The low extent of swelling for ODPA-based PEIs, between 3 and 4% measured up to 50 bar, as well as high CO_2/CH_4 selectivities (between 40 and 60) at a mixed gas feed pressure of 40 bar, show that these materials are of potential interest for CO_2 removal applications at elevated pressures. ODPA-P1, see Fig. 1, showed a decrease in CH_4 permeability with increasing pressure, which is a desirable property indicating that upon equal CO_2 permeability, the selectivity for separation increased with increasing pressure. Increasing the number of *para*-arylether units in the diamine moiety reduced the CO_2/CH_4 selectivity [21]. This simple prototypical PEI motivated us to investigate how subtle changes in the PEI main-chain affect gas transport properties and CO_2 swelling behavior. The role of the dianhydride structure, *i.e.* rigid versus flexible, were investigated as well as the aryloxy-substitution pattern (*para*, *meta* or *ortho*) of the diamine moiety.

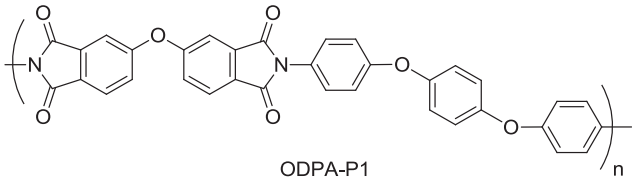

ODPA-P1

Fig. 1. Molecular structure of polyetherimide ODPA-P1 [21].

In order to understand the relationship between the PEI main-chain structure and its membrane gas separation (CO_2/CH_4) performance we have synthesized a systematic series of 12 PEI model compounds. All the diamine moieties are based on either *para*-, *meta*-, or *ortho*-based aryl ether units, which act as “flexible” spacer units between the terminal *para*-phenylamine functionalities (Fig. 2). Three diamines were chosen for this study: 1,4-bis(4-aminophenoxy)benzene (P1), 1,3-bis(4-aminophenoxy)benzene (M1) and 1,2-bis(4-aminophenoxy)benzene (O1). Changing the exocyclic bond angle in this 3-ring diamine changes the PEI main-chain from a more linear to a more bend conformation that significantly affects the chain flexibility. In addition, the (local) electrostatic dipole moment changes as the oxygen atoms move closer to one another when moving from a *para*- to an *ortho*-substitution pattern.

Furthermore, four different dianhydride moieties have been selected with the aim to systematically change the flexibility of the polymer backbone and the non-equilibrium excess free volume of the subsequent PEI membranes. The selected dianhydrides, listed from flexible to rigid, include: 3,3′,4,4′-oxydiphthalic dianhydride (**ODPA**), 3,3′,4,4′-benzophenonetetracarboxylic dianhydride (**BTDA**), 3,3′,4,4′-biphenyltetracarboxylic dianhydride (**BPDA**) and pyromellitic dianhydride (**PMDA**). The dianhydrides and their PEI main-chain structures are shown in Fig. 2.

2. Experimental

2.1. Materials

1,2-bis(4-aminophenoxy)benzene (O1) was synthesized according to a standard nucleophilic displacement reaction as shown in Scheme 1 [22]. All other start materials were purchased from commercial sources and used as received unless stated otherwise. Dianhydrides ODPA, BTDA, BPDA and PMDA were purchased from TCI Co. Ltd. and dried prior to use overnight in a vacuum oven at 60 °C. Diamine P1 was purchased from ABCR, diamine M1 from TCI and N-Methyl-2-pyrrolidinone (NMP) was obtained from Acros Organics.

2.2. Characterization

The chemical structure of O1 diamine was confirmed by ^{1}H NMR (Bruker WM-400, 400 MHz) and ^{13}C NMR (Bruker WM-400, 100 MHz). All samples were dissolved in deuterated chloroform and the recorded spectra were referenced to the solvent ($CDCl_3$: ^{1}H 7.26 and ^{13}C 77.0 ppm) relative to TMS. For GC/MS analysis of O1, a Shimadzu GCMS-QP2010S gas chromatograph mass spectrometer was used, coupled with the GL Sciences Optic 3 high-performance injector. Separation of the evolved gases was achieved using a 30 m × 0.025 mm SGE forte BPX-5 capillary column operated at a He flow rate of about 1 mL/min. Software ATAS Evolution Workstation (ATAS GL International) controlled heating of the injection port of the GC from 50 °C to 300 °C in 5 min. The GC column oven was programmed from 50 °C, with a heating rate of 20 °C/min, to 300 °C (held for 30 min). LabSolutions data system, GCMSsolutions (Shimadzu) Postrun analysis software was used to integrate the peaks. Melting point of O1 was determined using a Leica DM LM optical microscope equipped with a Linkam TMS94 hot stage; heating rate was 5 °C/min.

Gel permeation chromatography (GPC) measurements of polyamic acids were performed on a Shimadzu Prominence GPC system equipped with two Shodex LF-804 columns. N-Methyl-2-pyrrolidone (NMP) with 5 mM of LiBr was used as eluent at a flow rate of 0.5 mL/min at 60 °C. Data analyses were performed with LabSolutions software using the refractive index detector data. Quantification was made based on

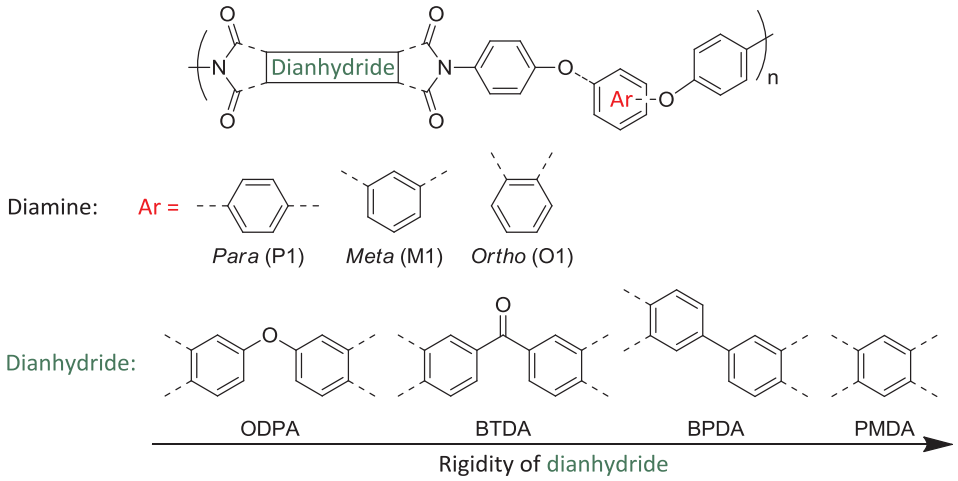

Fig. 2. Chemical structures of the prototypical PEI main-chain model systems that were used for this study (see also Table S1 in the Supporting information). The PEI main-chain varies from flexible to rigid and does not contain bulky side-groups or polar side-group functionalities.

polystyrene standard calibration. All polyamic solutions were filtered through a 0.45 µm PTFE filter prior to a GPC run.

Thermogravimetric analysis (TGA) was performed on a Perkin Elmer Pyris diamond TG/DTA under a nitrogen atmosphere and a scan rate of 10 °C/min. Sample films were cleaned and degreased with ethanol and dried at 60 °C for 2 h. The thermal properties of our PEI films were determined by differential scanning calorimetry (DSC) using a PerkinElmer Sapphire DSC. Samples were heated at a rate of 20 °C/min under a nitrogen atmosphere ~ 450 °C, depending on the samples thermal stability range as determined by TGA. Polymer thin films were investigated using a dynamic mechanical thermal analyzer (DMTA) in the temperature range −100 °C to 400 °C, at a heating rate of 2.5 °C/min and at a frequency of 1 Hz under a nitrogen atmosphere. Approximate dimensions of films were 20 × 4 × 0.03 mm. All samples were dried in a vacuum oven at 60 °C for 1 h prior to testing.

To investigate the morphology of the PEI films (15–35 µm), wide-angle XRD experiments were conducted using a Bruker AXS D8 Discover X-ray diffractometer in transmission mode with Cu Kα as the radiation source. For every PEI film, four layers were fixed onto a support, with the film surface perpendicular to the beam direction. All experiments were performed at room temperature, the sample–detector distance was set at 6 cm and the exposure time was set to 10 min.

2.3. Monomer synthesis

1,2-bis(4-nitrophenoxy)benzene: A dried 1000 mL three-neck flask, equipped with a nitrogen inlet, a mechanical overhead stirrer and a Dean–Stark trap with reflux condenser, was charged with 9.38 g (0.085 mol) of 1,2-dihydroxybenzene (catechol), 23.54 g (0.170 mol) of finely ground K_2CO_3, 160 mL of toluene and 200 mL of dimethylacetamide. This mixture was heated and stirred at 135 °C for 1.5 h, after which the temperature was increased to 175 °C. The theoretical amount of water was collected in the Dean–Stark trap and removed together with the toluene. The reaction mixture, now dark colored, was cooled to room temperature and 24.03 g (0.170 mol) of 1-fluoro-4-nitrobenzene was added. This mixture was heated at 160 °C overnight. The reaction mixture was cooled to room temperature and precipitated in 600 mL of ice water. The solids were collected by filtration, washed with water and recrystallized twice from 96% ethanol. Yield 24.32 g (81%); mp: T_{onset} = 134 °C, T_{max} = 136 °C (135–136 °C) [23]. TLC: (9/1 hexane/ethyl acetate) t_r = 0.134 (one spot).

1,2-bis(4-aminophenoxy)benzene (O1). A 250 mL hydrogenation bottle was charged with 12 g (0.034 mol) of 1,2-bis(4-nitrophenoxy) benzene, 100 mL of dry THF, and 1.2 g of 10% palladium on carbon. After degassing with nitrogen for 20 min, the bottle was placed in a Parr hydrogenator, and the nitro group was reduced under hydrogen atmosphere at 50 psi for 5 h at room temperature, then the shaker was turned off and the mixture was left under the same conditions (pressure and temperature) overnight. The solution was filtered over silica gel and celite, and the THF was removed by rotary evaporation. Pure O1 was obtained after two recrystallizations from ethanol/water (90/10) as pale brown crystals. Yield: 7 g (71%); mp: T_{onset} = 132 °C, T_{max} = 136 °C (135–136 °C) [22]. TLC (9/1 hexane/ethyl acetate) t_r = 0 (one spot). ^{1}H NMR ($CDCl_3$, 400 MHz) δ (ppm): 3.46 (s, 4H), 6.63 (d, 4H, J = 8.4 Hz), 6.83 (d, 4H, J = 8 Hz), 6.89–6.96 (m, 4H); ^{13}C NMR ($CDCl_3$, 400 MHz) δ (ppm): 116.1, 119.2, 119.9, 123.1, 142.1, 148.7, 149.3.

2.4. Polymer synthesis

Polyamic acids of high molecular weight were prepared from the dianhydride and diamine monomers, in equimolar quantities, as 15 wt % solutions in NMP at 25 °C.

Preparation of ODPA-P1 15 wt% polymer film (representative

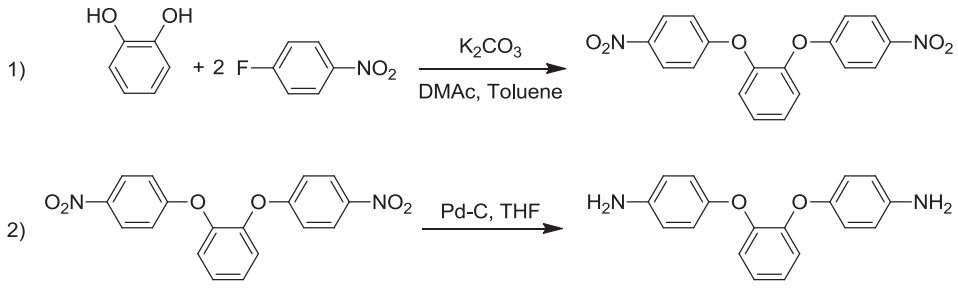

Scheme 1. Synthesis of 1,2-bis(4-aminophenoxy)benzene (O1).

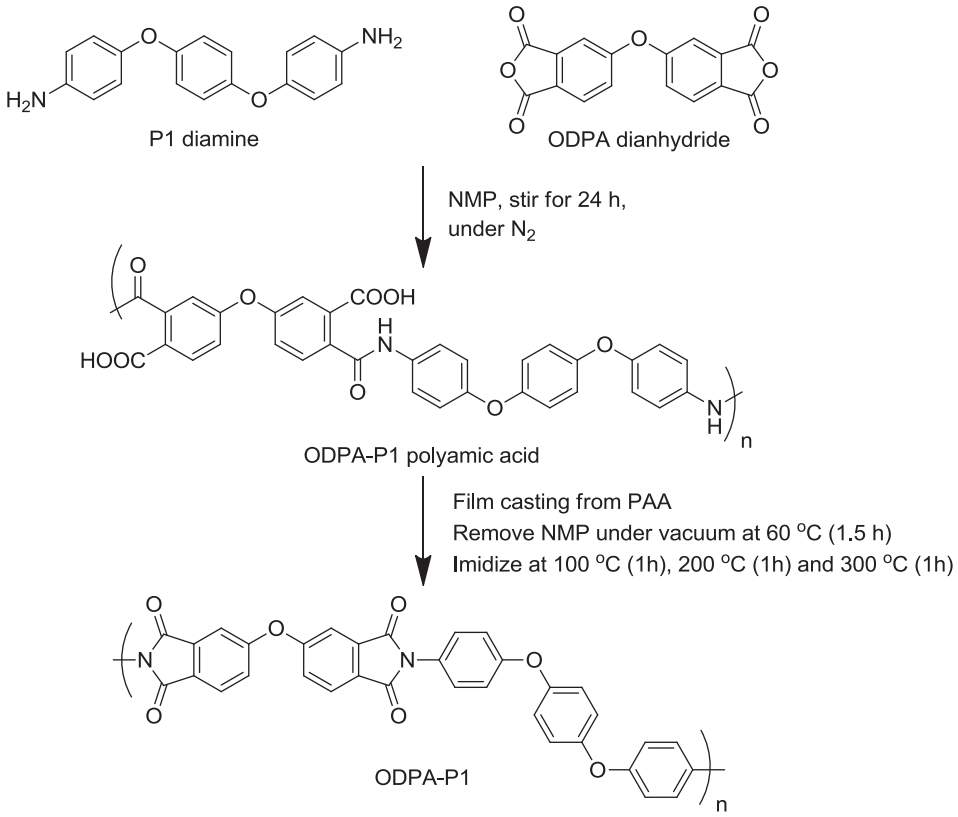

Scheme 2. Polymerization procedure used to prepare an ODPA-P1 free-standing film.

procedure, Scheme 2*):* A dry 50 mL one-neck round-bottom flask was charged with 1.498 g (5.12 mmol) of 1,4-bis(4-aminophenoxy)benzene (P1) and 18 mL of dry NMP (water content < 0.005%) was added. This solution was then stirred for 5 min, under a dry nitrogen flow, at room temperature with a magnetic stirrer at 120 rpm until the diamine monomer was dissolved. After this step the polymerization was initiated by adding 1.589 g (5.12 mmol, an equimolar amount) of 3,3′,4,4′-oxydiphthalic dianhydride (ODPA), and the walls of the flask were washed with 2 mL of NMP. Polymerization was allowed to continue for 24 h. under a nitrogen atmosphere, stirring at 90 rpm.

Film preparation. In order to remove any present solids, the polyamic acid solution was filtered using a Sartorius pressure filter (PTFE, pore size 0.45 µm). The resulting filtered solution (15 wt%) was degassed to remove bubbles and then cast with a doctor-blade onto a clean, dry glass plate (wet film thickness ~0.6 mm) and placed in a clean vacuum oven at 60 °C for 1.5 h. Films were thermally imidized by heating to 100 °C for 1 h, 200 °C for 1 h, and 300 °C for 1 h. After an overnight cooling to 25 °C, the film was released from the glass plate by placing it in lukewarm water. Using this procedure, all PEIs were obtained as free-standing films with thicknesses varying from 10 µm to 35 µm.

2.5. Gas permeation measurements

Gas permeation experiments were performed to evaluate the CO_2/CH_4 separating ability of our PEI membranes using the constant volume variable pressure method with vacuum at the permeate side as described elsewhere [24]. The N_2, CO_2, and CH_4 permeabilities of the PEI films as well as the separation performance of the membrane for a CO_2/CH_4 (50/50) mixture were measured as function of feed pressure at constant temperature. Experiments were performed in two permeation cells simultaneously, both operating at the same pressure (four different pressures used were 10, 20, 30 and 40 bar). Permeability coefficients were calculated from the steady-state pressure increase in time in a calibrated volume at the permeate side with Eq. (1):

$$\frac{P}{l} = \frac{V_c \cdot 273.15 \cdot (P_{pt} - P_{p0})}{A \cdot T \cdot \frac{(P_{ft} + P_{f0})}{2} \cdot 76 \cdot t} \quad (1)$$

where the ideal gas law is assumed to be valid and t (s) is the measurement time, P_{pt}, P_{ft} (bar) the pressure at the permeate and feed side at time t, P_{p0} and P_{f0} are the permeate and feed pressure at $t = 0$, T (K) is the temperature, V_c (cm^3) the calibrated permeate volume, and A (cm^2) the total membrane area [25]. The gas permeance P/l is expressed in gas permeation unit, GPU, *i.e.* 10^{-6} cm^3/cm^2 s cmHg. Multiplying the gas permeance with the membrane thickness, l (µm), gives the permeability coefficient in Barrer (1 Barrer = 10^{-10} $(cm^3_{STP})\cdot cm \cdot cm^{-2}\, s^{-1} \cdot cmHg^{-1}$). As a correction for non-ideal behavior, partial pressures were replaced by their corresponding fugacities. All the gas permeation experiments were performed at 35 °C.

Alternating nitrogen and CO_2/CH_4 gas permeation measurements were performed on the same membrane samples. The pressure of the nitrogen feed was kept constant at 5 bar to investigate plasticization effects. The pressure of the CO_2/CH_4 feed was increased from 10 to 20, 30 and 40 bar. In experiments with the CO_2/CH_4 (50/50) binary mixture, for each feed pressure, the flow rate of the retentate was kept constant and equal to 30 cm^3 (STP)/min in order to achieve a uniform feed composition over the membranes. Sufficient permeate was collected to reach a signal/noise (S/N) ratio of at least 10. Mixed gas selectivity was calculated with Eq. (2):

$$\alpha_{CO_2/CH_4} = \frac{y_{CO_2}/y_{CH_4}}{x_{CO_2}/x_{CH_4}} \quad (2)$$

where y and x are the concentrations of components in the permeate stream and feed stream, respectively.

For gas permeation experiments, the detailed experimental protocol consisted of the following steps:

Table 1
Molecular weight (M_n, and M_w) data and polydispersity indices as determined by GPC and inherent viscosities (η_{inh}) of the polyamic acids.

Polymer	M_n (g/mol)	M_w (g/mol)	PDI = M_w/M_n	η_{inh}[a] (dL/g)
ODPA-P1	64,000	119,000	1.9	0.78
BTDA-P1	109,000	212,000	2.0	0.89
BPDA-P1	102,000	191,000	1.9	1.11
PMDA-P1	108,000	154,000	1.4	2.00
ODPA-M1	63,000	152,000	2.4	0.98
BTDA-M1	87,000	169,000	1.9	0.89
BPDA-M1	59,000	153,000	2.6	1.09
PMDA-M1	69,000	174,000	2.5	1.70
ODPA-O1	53,000	104,000	2.0	0.72
BTDA-O1	119,000	331,000	2.8	1.03
BPDA-O1	84,000	364,000	4.3	1.15
PMDA-O1	97,000	296,000	3.1	1.03

[a] Inherent viscosities of the polyamic acids were measured using an Ubbelohde viscometer at room temperature, at a concentration of 0.5 g/dL in NMP.

1. Determine pure N_2 permeability at 5 bar;
2. Switch to mix feed of 10 bar;
3. Determine the separation properties (after at least 8 h);
4. Overnight membrane degassing with N_2 (5 bar);
5. Repeat Step 2 with increased feed pressure by 10 bar.

The high-pressure permeation unit was fully automated and controlled by means of Lab View Software. The temperature was kept constant at 35 °C. Two membranes were measured simultaneously and their permeabilities were determined separately by GC.

3. Results and discussion

3.1. Viscosity and gel permeation chromatography measurements

The molecular weights of the polyamic acid intermediates, measured using GPC, are listed in Table 1. The actual GPC curves are shown in the Supporting information (Fig. S1).

High molecular weight polyamic acids could be prepared without difficulty, with number average molecular weights in the range of ~60,000 to ~120,000 g/mol. As all polyamic acids were synthesized from the same procedures and under the same conditions, the variations in the molecular weight are thought to come from the differences in the monomer purity and reactivity. All P1-based polyamic acids show an unimodal molecular weight distribution (Fig. S1 in the SI) and the highest number average molecular weights (Table 1). With the exception of PMDA-M1, PMDA-O1 and BPDA-O1, all GPC curves show a unimodal molecular weight distribution.

Inherent viscosities of the polyamic acids were between 0.7 and 2.0 dL/g. Tough, flexible and easy-to-handle films were obtained after thermal imidization. All polyamic acid solutions were prepared at 15 wt % solids, however this concentration proved to be difficult for casting a useful PMDA-P1 film. Thus, this polyamic acid was prepared at 10 wt% solids in order to cast a useful polyamic acid film. The viscosity of this solution was 2.0 dL/g. Although the other two PMDA-based polyamic acids exhibited inherent viscosities of 1.7 and 1.03 dL/g, respectively, the fully imidized PMDA-M1 and PMDA-O1 films appeared highly crystalline and very brittle in nature. The films had to be handled with care and did not form good defect-free membranes. The polymerization of ODPA with all three diamines resulted in polyamic acids with the lowest inherent viscosity. None of the fully imidized films were soluble in NMP at 25 °C (10 mg polymer/mL).

3.2. Dynamic thermogravimetric analysis (TGA)

The thermal stability of the PEI films was investigated by dynamic thermogravimetric analysis (TGA). This provides information with respect to the polymer decomposition temperature, the temperature at which a weight loss of 5% occurs ($T_{5\%}$). The resulting thermograms, showing polymer weight as a function of temperature, are shown in the Supporting information (Fig. S2) and the values for $T_{5\%}$ and char yield are presented in Table 2.

All 12 PEIs show a gradual decrease in weight as a function of temperature up to ~500 °C (Fig. S2 in the Supporting information). The weight loss below 500 °C is due to outgassing of low molecular weight species such as moisture and solvent (NMP). Above 500 °C, the PEI films degrade due to thermal decomposition. The values reported here are typical for all-aromatic PEIs [22]. As the PEI-based membranes will operate at or slightly above 25 °C the thermal stability of this PEI-series

Table 2
Dynamic thermogravimetric analysis, (thermo)mechanical properties and morphology of the fully imidized polyetherimide films.

Polymer	TGA[a]		DSC[b]		DMTA[b]		XRD	
	5% weight loss (°C)	char yield at 595 °C (%)	T_g (°C)[c]	T_m (°C)[d]	T_g (°C)[e]	E' (GPa)[f]	morphology[g]	ϕ_c (%)[h]
ODPA-P1	531	70	248		248	4.5	Am	
BTDA-P1	509	71	286		302	6.5	SC	18
BPDA-P1	542	76	272	457	276	5.4	SC	6
PMDA-P1	533	70			321	4.8	SC	19
ODPA-M1	530	71	221		221	8.1	Am	
BTDA-M1	510	71	238	342	261	6.6	SC	6
BPDA-M1	549	81	236	394	242	4.0	SC	3
PMDA-M1[i]	540	72			318	4.7	SC	11
ODPA-O1	508	73	217		226	4.9	Am	
BTDA-O1	504	70	239		238	5.2	Am	
BPDA-O1	520	73	248		248	4.9	Am	
PMDA-O1[i]	509	74			302	4.1	SC	4

[a] Heating rate 10 °C/min and nitrogen atmosphere.
[b] DSC (second heating) and DMTA data were collected using a heating rate of 20 and 2.5 °C/min, respectively.
[c] T_g is reported at the inflection point.
[d] T_m is reported as the peak temperature.
[e] T_g is determined at the maximum of the loss modulus (E″).
[f] Value at 30 °C.
[g] Morphology: SC = semi-crystalline; Am = amorphous.
[h] ϕ_c is the degree of crystallinity determined by XRD.
[i] Brittle film.

will not be an issue.

3.3. Differential scanning calorimetry (DSC)

The T_g and T_m data are summarized in Table 2 and the DSC curves, second heats only, are shown in Supporting information (Fig. S3). Both P1- and M1-series gave three semi-crystalline and one amorphous polymer film, while the O1-series gave one semi-crystalline film. However, since the DSC measurements were performed up to a temperature limit determined by the thermal stability of each polymer as determined by TGA measurements, not all of the melting endotherms are observable by DSC as they may overlap with the polymer degradation temperature. We were unable to detect a T_g for the PMDA-based films by DSC.

For the P1- and M1-based PEI films we observed the following trend in T_g: PMDA > BTDA > BPDA > ODPA. The trend for the O1-based PEIs is similar except for the fact that the T_g of BPDA-O1 > BTDA-O1. As anticipated, the more rigid PMDA-based PEIs exhibit the highest T_g values and the flexible ODPA-based PEIs display the lowest T_g values. BPDA-P1, BTDA-M1 and BPDA-M1 are the only 3 films exhibiting an accessible melting point. The melting points for semi-crystalline BPDA-P1, BTDA-M1 and BPDA-M1 are 457 °C, 342 °C and 394 °C respectively, and these results are in agreement with previously reported T_m values [22]. It has to be noted that the onset of the melting endotherm of BPDA-P1 is observed at ~450 °C. However, due to restrictions of the upper temperature limit, (determined by TGA) the melt event could not be recorded.

3.4. Dynamic mechanical thermal analysis (DMTA)

The DMTA results show the values for the storage modulus (E') and T_g as determined at the maximum of the loss modulus (E″) (Table 2). All PEI membrane films show storage moduli (E′) of 4–8 GPa, which is typical for all-aromatic PEIs films [21]. The T_g values determined by DMTA correspond well with the ones observed by DSC. All DMTA curves are shown in Supporting information (Fig. S4). With the exception of the PMDA-based PEIs, all films show clear T_g events as determined at the max of E″. The same is true for the β-transitions, which can clearly be observed between 80 and 110 °C for all films with the exception of the PMDA-based films. The PMDA-based polyimides generally possess a higher T_g than the corresponding BPDA- and BTDA-based analogues while the dilution of the imide content by the insertion of an ether linkage into the dianhydride (ODPA) significantly decreased the T_g. By replacing the central *para*-aryloxy unit with *meta*- or *ortho*-aryloxy units results in a decrease in T_g following the trend in the order P1 > M1 > O1.

3.5. Film morphology, X-ray diffraction (XRD)

Wide-angle XRD analysis was performed on all 12 PEI films (thickness of 15–35 μm) and the results are summarized in Table 2. All XRD spectra are shown in the Supporting information (Fig. S5). All three ODPA-based films are fully amorphous and all three PMDA-based films are semi-crystalline, with the degree of crystallinity decreasing in the order P1 > M1 > O1. This indicates that the more linear structures pack better, with the kinked structure of O1 only allowing a small degree of crystallinity (4%) in PMDA-O1. By comparing the ratio of the area under the crystalline peaks to the total area of the curve, the degree of crystallinity in the films was quantified. PMDA-P1 shows the highest degree of crystallinity of 19%, followed by BTDA-P1 and BPDA-P1 with values of 18% and 6%, respectively. XRD analysis of the M1-based films shows an identical trend in crystallinity, with PMDA-M1 displaying the highest degree of crystallinity (11%), followed by BTDA-M1 (6%) and BPDA-M1 (3%). Within the O1-based series, only PMDA-O1 shows a small degree of crystallinity (4%). Characteristic peaks corresponding to the lengths of polymer repeating units are observed for all three PMDA-based films and two BTDA-based films. In the XRD spectrum for PMDA-P1 (Fig. S5-A), the diffraction peak at $2\theta = 4.25^\circ$ corresponds to the repeat unit length of 20.8 Å, and for BTDA-P1 the diffraction peak at $2\theta = 3.49^\circ$ agrees with the length of repeat unit of 25.3 Å. For PMDA-M1 (Fig. S5-B) a diffraction peak at $2\theta = 4.21^\circ$ corresponds to the length of 21 Å and for BTDA-M1 the peak at $2\theta = 3.61^\circ$ corresponds to a repeat unit length of 24.5 Å. In case of PMDA-O1 (Fig. S5-C) the peak is not sharp enough for determining the length of the repeat unit. The polyimides derived from rigid, rod-like dianhydride (PMDA) showed the higher crystalline tendency and higher T_g, also shown by Hsiao et al. [26].

3.6. Gas separation performance

Polymers PMDA-M1 and PMDA-O1 were too brittle to handle and therefore they could not be tested as gas separation membranes in a membrane cell. Attempts were made but significant leaks were observed and therefore the results were omitted.

The permeability of CO_2 is greater than that of CH_4 due to its significantly higher diffusivity and higher solubility in the polymer [27]. In this gas pair the CH_4 permeability is very low and therefore the focus in our discussion will be on the more significant CO_2 permeability values. Fig. 3 shows the CO_2 permeabilities of our 10 PEI membranes as a function of the CO_2 fugacity at 35 °C, grouped by the diamine moiety for sake of clarity. All measurements were performed *in duplo*.

In Fig. 3A three membranes, ODPA-P1, BTDA-P1 and BPDA-P1, show a very slight decrease in CO_2 permeability with increasing feed pressure, while PMDA-P1 shows typical plasticization behavior with a minimum in permeability. This decrease in permeability at lower pressures comes from the decreasing solubility with increasing pressure, following the predicted behavior of the dual-mode sorption model [27,28]. As the CO_2 pressure increases further, more CO_2 is sorbed into the polymer matrix causing increased chain mobility (an increase in gas diffusion) and plasticization [12,29–31]. This leads to an upward inflection in permeability with increase in pressure. The highest permeability is observed for the PMDA-P1 membrane, going from 1.6 to 1.9 Barrer in the applied pressure range, twice as high as for the other three PEI membranes. The other three polymers do not show plasticization, the ODPA-P1 membrane shows the best performance with an average CO_2 permeability around 0.6 Barrer over the applied pressure range. Performance of the BTDA-M1 and BPDA-M1 membranes appears to be identical, with overlapping low values for CO_2 permeability around 0.1 Barrer (Fig. 3B). ODPA-M1 shows a slightly higher CO_2 permeability value of 0.3 Barrer. However, this membrane also suffers from plasticization. ODPA-O1 and BTDA-O1 appear to be resistant to CO_2 plasticization and show permeabilities of 0.5 and 0.32 Barrer respectively. Interestingly, BPDA-O1 shows a high initial permeability of 1.3 Barrer but this drops rapidly to 0.7 Barrer with increasing pressure, this initial compression would likely be followed by plasticization if higher pressures were applied.

In both ODPA- and BTDA-based membranes a trend is visible. Permeability of CO_2 for ODPA- and BTDA-based membranes decreases slightly in the order P1 > O1 > M1 and remains steady throughout the measurements with the increasing mixed feed pressure up to 40 bar (17 bar of CO_2 fugacity). Therefore, if only looking at permeability, up to 40 bar, these six ODPA- and BTDA-based membranes seem to be resistant to plasticization, with CO_2 permeabilities remaining steady when the CO_2 pressure increases.

In gas separation, the phenomenon of penetrant induced plasticization is an undesirable side-effect. Since transport of the “slow” penetrant, CH_4 in our case, is being more affected, an overall loss in separation performance is observed. The BPDA-O1 membrane displays a drop in permeability at increasing pressure. The permeability approaches a minimum and it might increase again with further increase in pressure, likely resulting in a typical plasticization curve with the lowest value in permeability certainly above 40 bar of mixed feed

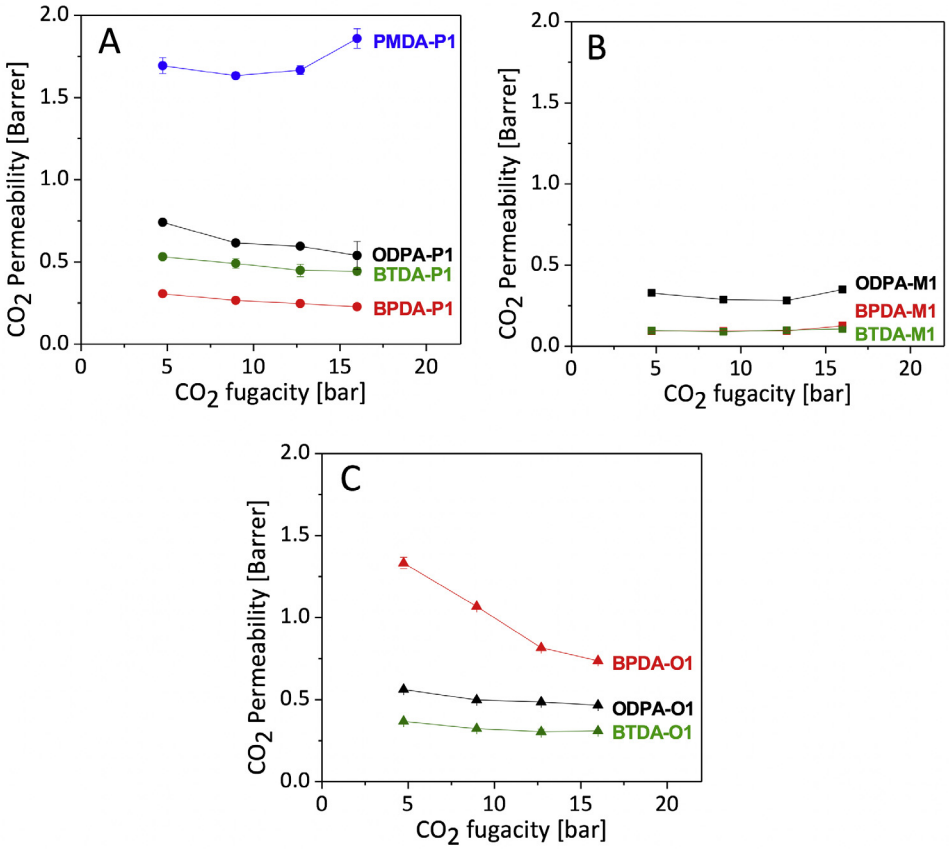

Fig. 3. CO_2 permeability as function of the CO_2 fugacity at 35 °C for (A) P1-series, (B) M1-series and (C) O1-based membrane series. Feed mixed gas: CO_2/CH_4 (50/50 vol%).

(17 bar of CO_2 fugacity). In this particular case, the permeability drops from 1.3 to 0.7 Barrer. With the other two diamines the permeability is relatively lower and remains stable up to 40 bar. The semi-crystalline BTDA-M1 and BPDA-M1 membranes show the lowest CO_2 permeabilities and are the least permeating of the 10 membranes reported here.

The gas separating performance of the 10 PEI membranes is shown in Fig. 4. The CO_2/CH_4 selectivities as a function of the gas partial pressure are presented and grouped by diamine moiety. With increasing pressure, we do not observe large differences in selectivity for the P1-based membranes, as shown in Fig. 4A. Three membranes show very similar values for selectivity at a feed pressure of 10 bar, selectivity of approximately 47. Moreover, they also show stable permeability values in the applied pressure range, thus with both CO_2 permeability and selectivity remaining steady, these membranes show resistance to plasticization which can be related to their relatively high T_g values. The selectivity values of the high-crystalline PMDA-P1 are significantly lower than for the other three films at any point. Having the highest value for permeability, it is expected for the PMDA-P1 membrane to have the lowest selectivity, due to the trade-off relationship between permeability and selectivity. The selectivities of ODPA-P1, BTDA-P1 and BPDA-P1 remain relatively constant at all feed pressures, with values between 42 and 48. Regardless of the slight decrease in selectivity for BTDA-P1 and BPDA-P1, these materials still have a selectivity of ~42 at a total feed pressure of 40 bar, which is much higher than the selectivity of the commercially available polyimide Matrimid®. However, their CO_2 permeabilities of less than 1 Barrer are very low compared to Matrimid®, which is reported to exhibit a selectivity of ~30 and CO_2 permeability of ~7 Barrer at 35 bar at the same temperature and a similar feed composition [32].

All three M1-based membranes show higher selectivity values than the P1-based membranes, again an example of the permeability/selectivity trade-off (Fig. 4B). With increased pressure however, all three membranes show a drop in selectivity from 58 to 48. This suggests plasticization behavior, but we cannot confirm without extending this study to even higher pressures.

The ODPA-O1 and BTDA-O1 membranes display the same undesirable decrease in selectivity behavior as the M1-based membranes, with their high values of selectivity dropping significantly as the feed pressure is increased to 20 bar. Selectivity values of the BPDA-O1 membrane remain high at 70 regardless of the pressure increase, however, CO_2 permeability drops significantly after the feed pressure is increased signifying plasticization behavior. This high selectivity value and permeability of 1.3 Barrer could make BPDA-O1 and interesting membrane for applications up to 10 bar and could be a promising candidate for additional ageing studies.

Fig. 5 shows our data contrasted with literature values available for similar PI and PEI membranes, with respect to permeability and CO_2/CH_4 selectivity. Robeson's upper bounds, as reported in 1991 and 2008, are added for reference purposes. Details and operating conditions of the data points shown in Fig. 5 are listed in Table S2 (Supporting information). Mixed gas separation performance of membranes at 10 bar of total pressure was used for comparison. Due to a lack of literature information on the mixed gas data, the pure gas data at low pressures were also included for comparison.

The permeability and selectivity of our PEI membranes are comparable to literature values. All 10 membranes show higher selectivity than that of commercially available polyimide Matrimid® but at the same time their permeabilities are lower, which is due to the permeability/selectivity trade-off relationship. Subtle changes in the backbone don't seem make a significant difference in gas separating performance. A higher permeability for PMDA-P1 is in line with other

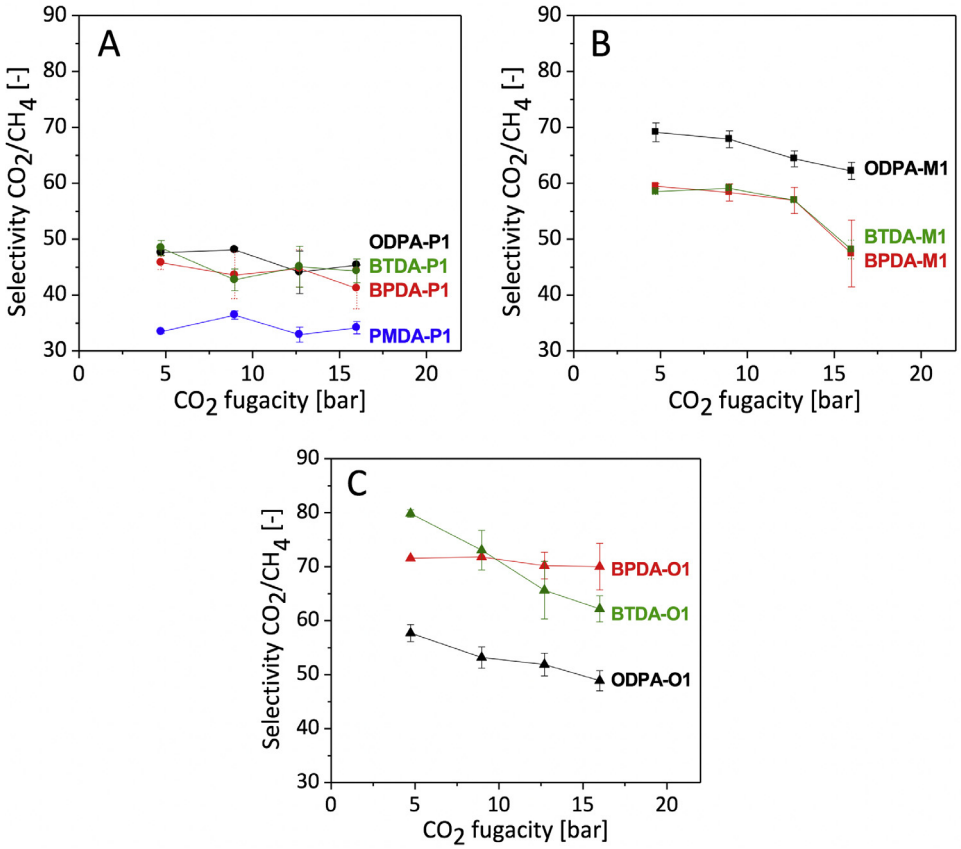

Fig. 4. CO_2/CH_4 selectivity as a function of the CO_2 fugacity for (A) The P1-series, (B) The M1-series and (C) The O1-based membrane series. Feed mixed gas: CO_2/CH_4 (50/50 vol%).

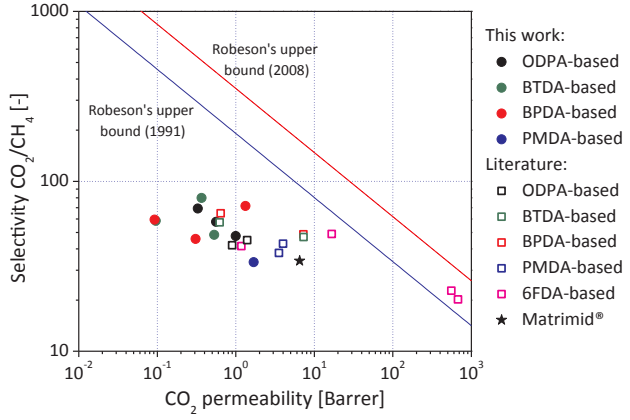

Fig. 5. Comparative study of P(E)I membranes for CO_2/CH_4 gas separation.

PMDA-based membranes, with their selectivities being 30 to 40. ODPA- and BTDA-based membranes show higher selectivities than 6FDA-based membranes, which have bulky $-CF_3$ groups that result in very high permeability values. Both flexible (–O–) and bulky ($-CF_3$) groups combined in the backbone could lead to higher permeabilities as well as higher selectivity.

4. Conclusions

A homologous series of 12 poly(etherimide)s based on 4 different aromatic dianhydrides and 3 aromatic diamines was prepared with the aim to understand the relationships between the polyetherimide main-chain structure and their performance as gas separation membranes. As gas separation membranes, these poly(etherimide)s show low values for permeability, high selectivity, resistance to plasticization and stable high-pressure performance. The highest permeability was observed for the semi-crystalline PMDA-P1 membrane, going up to ~2 Barrer in the applied pressure range, which is twice as high as for the other P1-based membranes. Unfortunately, the CO_2 permeability curve of PMDA-P1 indicates plasticization behavior. Of the other P1 membranes, not suffering from plasticization, the amorphous ODPA-P1 shows the best performance with an average CO_2 permeability around 0.6 Barrer throughout the applied pressure range. The selectivities of ODPA-P1, BTDA-P1 and BPDA-P1 membranes remain relatively constant at all feed pressures, with values between 42 and 48, making them attractive candidates for further high-pressure studies. All M1-based membranes show a drop in selectivity values from 58 to 48 with increasing pressure. For all ODPA- and BTDA-based membranes a trend could be identified in which the permeability increases slightly in the order P1 > O1 > M1. The permeability remains stable up to 40 bar, which is evidence that ODPA- and BTDA-based membranes do not suffer from plasticization. This study has yielded two interesting amorphous PEI membranes that need to be investigated in more detail. The OPDA-P1 membrane, which exhibits high selectivity and resistance to plasticization up to 40 bar and the BPDA-O1 membrane. The latter is of interest because of its high selectivity (70) and permeability (1.3 Barrer). In conclusion, we believe that the PEI series presented in this paper will aid in designing future generations PEI-based gas separation (CO_2/CH_4) membranes.

Acknowledgements

This research is funded by the Dutch Polymer Institute (DPI) under project #715. The authors would like to thank the European Commission – Education, Audiovisual and Culture Executive Agency

(EACEA) for funding a part of this research under the program named Erasmus Mundus Doctorate in Membrane Engineering – EUDIME (FPA N° 2011-0014).

Appendix A. Supplementary material

Supplementary data associated with this article can be found, in the online version, at https://doi.org/10.1016/j.seppur.2018.08.006.

References

[1] W.J. Koros, G.K. Fleming, Membrane-based gas separation, J. Membr. Sci. 83 (1993) 1–80.
[2] C.E. Powell, G.G. Qiao, Polymeric CO_2/N_2 gas separation membranes for the capture of carbon dioxide from power plant flue gases, J. Membr. Sci. 279 (2006) 1–49.
[3] S. Basu, A.L. Khan, A. Cano-Odena, C. Liu, I.F.J. Vankelecom, Membrane-based technologies for biogas separations, Chem. Soc. Rev. 39 (2010) 750–768.
[4] B.D. Bhide, A. Voskericyan, S.A. Stern, Hybrid processes for the removal of acid gases from natural gas, J. Membr. Sci. 140 (1998) 27–49.
[5] G.T. Rochelle, Amine scrubbing for CO_2 capture, Science 325 (2009) 1652–1654.
[6] K. Simons, Membrane Technologies for CO_2 Capture, PhD Thesis University of Twente, 2010.
[7] S. Matteucci, Y. Yampolskii, I. Pinnau, B.D. Freeman, Transport of gases and vapors in glassy and rubbery polymers, in: Y. Yampolskii, I. Pinnau, B.D. Freeman (Eds.), Materials Science of Membranes for Gas and Vapor Separation, John Wiley & Sons, Chichester, UK, 2006, pp. 1–48.
[8] I. Rose, M. Carta, R. Malpass-Evans, M. Ferrari, P. Bernardo, G. Clarizia, J.C. Jansen, N.B. McKeown, Highly permeable benzotriptycene-based polymer of intrinsic microporosity, ACS Macro Lett. 2 (2015) 4–7.
[9] L.M. Robeson, The upper bound revisited, J. Membr. Sci. 320 (2008) 390–400.
[10] L.M. Robeson, Correlation of separation factor versus permeability for polymeric membranes, J. Membr. Sci. 62 (1991) 165–185.
[11] A.Y. Alentiev, K.A. Loza, Y.P. Yampolskii, Development of the methods for prediction of gas permeation parameters of glassy polymers: polyimides as alternating co-polymers, J. Membr. Sci. 167 (2000) 91–106.
[12] P.S. Tin, T.S. Chung, Y. Liu, R. Wang, S.L. Liu, K.P. Pramoda, Effects of cross-linking modification on gas separation performance of Matrimid membranes, J. Membr. Sci. 225 (2003) 77–90.
[13] T. Visser, N. Masetto, M. Wessling, Materials dependence of mixed gas plasticization behavior in asymmetric membranes, J. Membr. Sci. 306 (2007) 16–28.
[14] J. Xia, T. Chung, D.R. Paul, Physical aging and carbon dioxide plasticization of thin polyimide films in mixed gas permeation, J. Membr. Sci. 450 (2014) 457–468.
[15] J.N. Barsema, G.C. Kapantaidakis, N.F.A. van der Vegt, G.H. Koops, M. Wessling, Preparation and characterization of highly selective dense and hollow fiber asymmetric membranes based on BTDA-TDI/MDI co-polyimide, J. Membr. Sci. 216 (2003) 195–205.
[16] C. Staudt-Bickel, W.J. Koros, Improvement of CO_2/CH_4 separation characteristics of polyimides by chemical crosslinking, J. Membr. Sci. 155 (1999) 145–154.
[17] J.D. Wind, C. Staudt-Bickel, D.R. Paul, W.J. Koros, Solid-state covalent cross-linking of polyimide membranes for carbon dioxide plasticization reduction, Macromolecules 36 (2003) 1882–1888.
[18] T. Merkel, B.D. Freeman, R.J. Spontak, Z. He, I. Pinnau, P. Meakin, A.J. Hill, Ultrapermeable, reverse-selective nanocomposite membranes, Science 296 (2002) 519–522.
[19] Y. Liu, R. Wang, T. Chung, Chemical cross-linking modification of polyimide membranes for gas separation, J. Membr. Sci. 189 (2001) 231–239.
[20] D. Ayala, A.E. Lozano, J. de Abajo, C. Garcia-Perez, J.G. de la Campaa, K.-V. Peinemann, B.D. Freeman, R. Prabhakar, Gas separation properties of aromatic polyimides, J. Membr. Sci. 215 (2003) 61–73.
[21] K. Simons, K. Nijmeijer, J.G. Sala, H. van der Werf, N.E. Benes, T.J. Dingemans, M. Wessling, CO_2 sorption and transport behavior of ODPA-based polyetherimide polymer films, Polymer 51 (2010) 3907–3917.
[22] T.J. Dingemans, E. Mendes, J.J. Hinkley, E.S. Weiser, T.L. StClair, Ortho-arylene substitutions: synthesis, characterization and liquid crystalline properties, Macromolecules (2008) 2474–2483.
[23] G.C. Eastmond, J. Paprotny, Methyl- and fluoro-substituted bis(4′-aminophenoxy) benzenes: a convenient method of synthesis, Synthesis 6 (1998) 894–898.
[24] T. Visser, G.H. Koops, M. Wessling, On the subtle balance between competitive sorption and plasticization effects in asymmetric hollow fiber gas separation membranes, J. Membr. Sci. 252 (2005) 265–277.
[25] D.M. Sterescu, D.F. Stamatialis, E. Mendes, J. Kruse, K. Rätzke, F. Faupel, M. Wessling, Boltorn-modified poly(2,6-dimethyl-1,4-phenylene oxide) gas separation membranes, Macromolecules 40 (2007) 5400–5410.
[26] S.-H. Hsiao, Y.-J. Chen, Structure–property study of polyimides derived from PMDA and BPDA dianhydrides with structurally different diamines, Eur. Polym. J. 38 (2002) 815–828.
[27] S.A. Stern, Polymers for gas separations: the next decade, J. Membr. Sci. 94 (1994) 1–65.
[28] D.R. Paul, Gas sorption and transport in glassy-polymers, Ber. Bunsenges. Phys. Chem. Chem. Phys. 83 (1979) 294–302.
[29] V. Stannett, The transport of gases in synthetic polymeric membranes—an historic perspective, J. Membr. Sci. 3 (1978) 97–115.
[30] T. Visser, M. Wessling, When do sorption-induced relaxations in glassy polymers set in? Macromolecules 40 (2007) 4992–5000.
[31] A. Bos, I.G.M. Punt, M. Wessling, H. Strathmann, CO2-induced plasticization phenomena in glassy polymers, J. Membr. Sci. 155 (1999) 67–78.
[32] D.F. Sanders, Z.P. Smith, R. Guo, L.M. Robeson, J.E. McGrath, D.R. Paul, B.D. Freeman, Energy-efficient polymeric gas separation membranes for a sustainable future: a review, Polymer 54 (2013) 4729–4761.